Supporting Information

NMP makes the Difference – Facilitated Synthesis of [FeFe] Hydrogenase Mimics

Stefan Benndorf[a], Philipp Buday[a], Benedikt Callies[a], Helmar Görls[a], Stephan Kupfer[b] and Wolfgang Weigand*[a,c]

[a] S. Benndorf, P. Buday, B. Callies, Dr. H. Görls, Prof. Dr. W. Weigand
Institute of Inorganic and Analytical Chemistry, Friedrich Schiller University Jena,
Humboldtstrasse 8, 07743 Jena, Germany
E-mail: wolfgang.weigand@uni-jena.de

[b] Dr. S. Kupfer
Institute of Physical Chemistry, Friedrich Schiller University Jena
Helmholtzweg 4, 07743 Jena, Germany

[c] Center for Energy and Environmental Chemistry Jena (CEEC Jena), Jena Center of Soft Matter, Friedrich Schiller University Jena,
Philosophenweg 7a, 07743 Jena, Germany

Materials and Methods

All solvents as well as commercially available compounds were purchased (Sigma-Aldrich, Acros, abcr, Alfa Aesar, TCI) and used as received without further purification. Toluene was dried and deoxygenated over Na metal. The NMR spectra were recorded with a Bruker Avance 400 MHz spectrometer. Chemical shifts are given in ppm relative to internal $SiMe_4$ or $CHCl_3$ (^1H, $^{13}C\{^1H\}$, $^{77}Se\{^1H\}$, $^{125}Te\{^1H\}$). IR spectra were measured with a Tensor 27 FT-IR spectrometer. Additionally, a Specac OMNI OTTLE cell was used for IR measurements in solution. DIPEI mass spectrometry (70 eV) was performed with a Finnigan MAT SSQ 710. UV-Vis spectroscopy was carried out at a Specord S600 A with 4- or 10-mm pathway cuvette.

Structure Determinations: The intensity data for the compound **2c** was collected on a Nonius KappaCCD diffractometer using graphite-monochromated Mo-K_a radiation. Data were corrected for Lorentz and polarization effects; absorption was taken into account on a semi-empirical basis using multiple-scans.[1] The structure was solved by intrinsic phases (SHELXT[2]) and refined by full-matrix least squares techniques against Fo^2 (SHELXL-2018[3]). All hydrogen atoms were included at calculated positions with fixed thermal parameters. MERCURY was used for structure representations.[4]

Molecular structure

Crystal Data for **2c**: $C_{10}H_{10}Fe_2O_8S_2$, Mr = 434.00 gmol^{-1}, red-brown prism, size 0.104 x 0.102 x 0.088 mm^3, triclinic, space group P $\bar{1}$, a = 9.9054(2), b = 12.9304(3), c = 14.3840(3) Å, α = 67.548(1), β = 75.695(1), γ = 72.133(1)°, V = 1602.78(6) Å^3 , T= -140 °C, Z = 4, $\rho_{calcd.}$ = 1.799 gcm^{-3}, μ (Mo-K_α) = 21.03 cm^{-1}, multi-scan, transmin: 0.6818, transmax: 0.7456, F(000) = 872, 23102 reflections in h(-12/12), k(-16/16), l(-18/18), measured in the range 1.754° ≤ Θ ≤ 27.484°, completeness Θ_{max} = 99.6%, 7304 independent reflections, R_{int} = 0.0373, 6376 reflections with $F_o > 4\sigma(F_o)$, 413 parameters, 0 restraints, $R1_{obs}$ = 0.0358, wR^2_{obs} = 0.0772, $R1_{all}$ = 0.0438, wR^2_{all} = 0.0815, GOOF = 1.054, largest difference peak and hole: 0.638 / -0.406 e Å^{-3}.

Exemplarily, Figure S1 and S2 show the molecular structure and atom numbering scheme of compound **2c**. The X-ray structure determination exhibits two symmetry-independent molecules A (Figure S1) and B (Figure S2). Both structures reveal the characteristic butterfly conformation of the [Fe_2S_2] cluster. The coordination sphere in the vicinity of each Fe atom can be described as a distorted octahedral with two *m*-bridging S atoms, and three terminal CO ligands. The Fe-Fe bond length of both structures (Fe_{1A}-Fe_{2A} 2.5332(5) Å, Fe_{1B}-Fe_{2B} 2.5184(5) Å) are in good agreement with comparable non-bridged dithiolato complexes.[5,6]

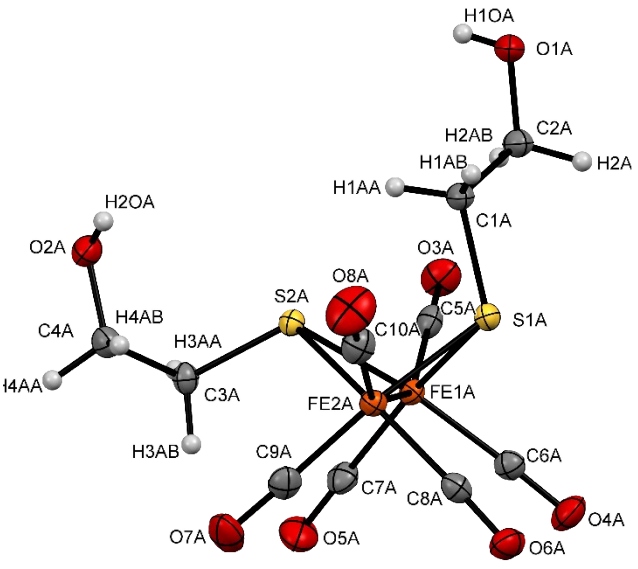

Figure S1. Molecular structure (A) and atom numbering of complex 2c. The ellipsoids represent a probability of 50 %, H atoms are drawn with arbitrary radii.

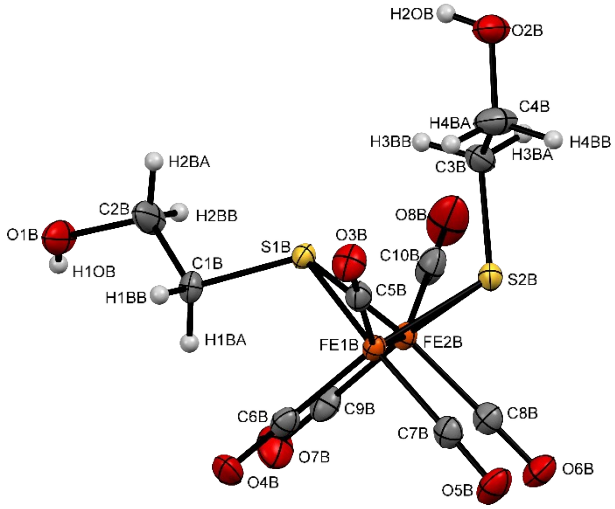

Figure S2. Molecular structure (B) and atom numbering of complex 2c. The ellipsoids represent a probability of 50 %, H atoms are drawn with arbitrary radii.

Crystallographic data (excluding structure factors) has been deposited with the Cambridge Crystallographic Data Centre as supplementary publication CCDC- 2205533 for **2c**. Copies of the data can be obtained free of charge on application to CCDC, 12 Union Road, Cambridge CB2 1EZ, UK [E- mail: deposit@ccdc.cam.ac.uk].

Synthesis

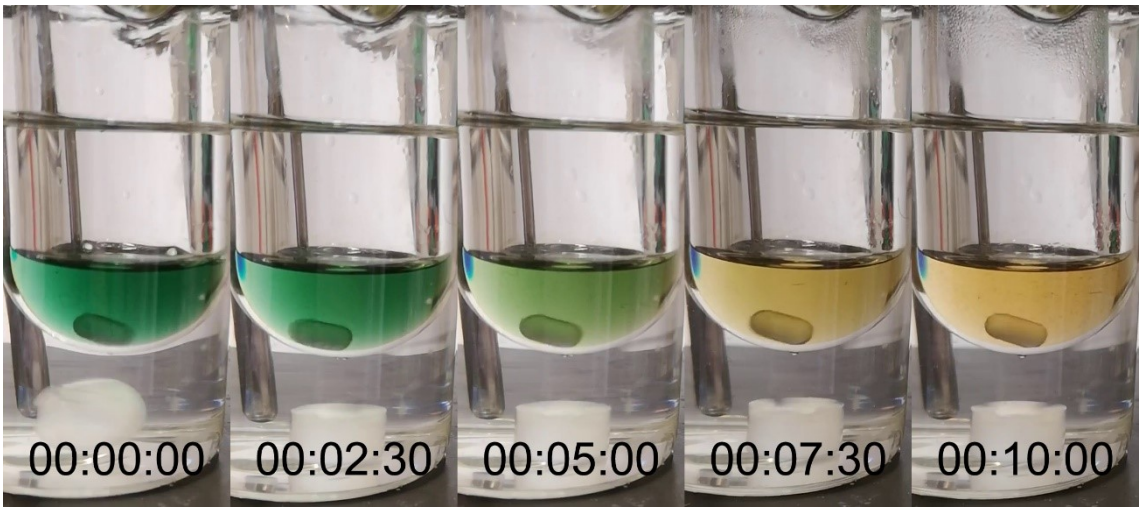

Figure S3. Photographs during the reaction of $Fe_3(CO)_{12}$ with equimolar amounts of 1a (toluene/NMP (10:1), $c \approx 2.2 \times 10^{-4}$ M) at 52 °C. Please keep in mind that the reaction time is extended in comparison to the experiment in Table 1, due to the less concentrated solution.

Experimental

Synthesis of diiron hexacarbonyl complexes **2a-n**

Precursors **1a-1n** (100 mg) were dissolved in toluene/NMP (10:1) mixture (11 mL) at 50 °C. After addition of $Fe_3(CO)_{12}$ (1 eq, 0.5 eq for **1c**) in one portion, the reaction was stirred until the dark green solution turned orange-red, monitored by TLC. Target compounds **2a-n** could be isolated as a red or brownish solids after purification via column chromatography (*n*-hexane/THF or *n*-hexane/ethyl acetate). All reaction times and isolated yields are depicted in Table 1. All complexes are known examples in the literature. Further characterization can be found in the cited original literature.

H_2ase mimics

2a[7]

^{1}H NMR (600 MHz, [D$_2$]DCM, 297 K, TMS) δ (ppm) = 2.16 (br s, 4H, CH_2S), 1.80 (br s, 2H, CH$_2$CH_2CH$_2$); MS (EI): m/z = 386 [M]$^+$, 358 [M-CO]$^+$, 330 [M-(CO)$_2$]$^+$, 302 [M-(CO)$_3$]$^+$, 274 [M-(CO)$_4$]$^+$, 246 [M-(CO)$_5$]$^+$, 218 [M-(CO)$_6$]$^+$; $\tilde{\nu}$ (CO) [cm^{-1}] = 2069, 2019, 1983, 1961, 1953; elemental analysis calcd. (%) for $C_9H_6Fe_2O_6S_2$: C 28.01, H 1.57, S 16.61; found: C 28.25, H 1.70, S 16.78.

2b[8]

^{1}H NMR (400 MHz, CDCl$_3$, 297 K, TMS) δ (ppm) = 3.19 – 3.07 (m, 1H, CH(OH)), 2.81 (dd, $^3J_{H\text{-}H}$ = 13.2, 4.1 Hz, 2H, CH_aH$_b$), 1.86 (d, $^3J_{H\text{-}H}$ = 5.6 Hz, 1H, OH), 1.56 – 1.48 (m, 2H, CH$_a$$H_b$); ^{13}C{^{1}H} NMR (101 MHz, CDCl$_3$, 297 K, TMS) δ (ppm) = 207.4, 72.9, 29.6; MS (EI): m/z = 374 [M-CO]$^+$, 346 [M-(CO)$_2$]$^+$, 318 [M-(CO)$_3$]$^+$, 290 [M-(CO)$_4$]$^+$, 262 [M-(CO)$_5$]$^+$, 234 [M-(CO)$_6$]$^+$; $\tilde{\nu}$ (CO) [cm^{-1}] = 2070, 2025, 1986, 1956; elemental analysis calcd. (%) for $C_9H_6Fe_2O_7S_2$: C 26.89, H 1.50, S 15.95; found: C 26.54, H 1.43, S 15.70.

2c and **2d**[9]

^{1}H NMR (600 MHz, CDCl$_3$, 297 K, TMS) δ (ppm) = 4.18 – 3.53 (m, 4H, CH_2S), 2.77 – 2.13 (m, 4H, CH_2O), 2.01 – 1.73 (m, 2H, OH); ^{13}C{^{1}H} NMR (151 MHz, CDCl$_3$, 297 K) δ (ppm) = 209.25, 208.36, 63.00, 41.25, 40.10, 27.65; MS (ESI positive mode): m/z = 456.841 (M + Na$^+$, calcd. 456.841); $\tilde{\nu}$ (CO) [cm^{-1}] = 2070, 2027, 2008, 1988, 1975, 1956.

2e[7]

^{1}H NMR (400 MHz, CDCl$_3$, 297 K, TMS) δ (ppm) = 2.57 (br s, 1H), 2.39 (m, 2H), 2.11 (br s, 1H), 1.86 (br s, 2H), 1.64-1.44 (m, 6H), 1.29 (br s, 1H); MS (EI): m/z = 486 [M]$^+$, 430 [M-(CO)$_2$]$^+$, 402 [M-(CO)$_3$]$^+$, 374 [M-(CO)$_3$]$^+$, 346 [M-(CO)$_5$]$^+$, 318 [M-(CO)$_6$]$^+$; $\tilde{\nu}$ (CO) [cm^{-1}] = 2069, 2023, 1981, 1955.

2f[10]

^{1}H NMR (400 MHz, CDCl$_3$, 297 K, TMS) δ (ppm) = 2.87 (dd, $^2J_{H\text{-}H}$ = 13.6, $^3J_{H\text{-}H}$ = 3.4 Hz, 2H, CH_aH$_b$), 2.17 (m, 1H, CH), 1.76 (t, J = 13.0 Hz, 2H, CH$_a$$H_b$); MS (EI): m/z = 402 [M-CO]$^+$, 374 [M-(CO)$_2$]$^+$, 346 [M-(CO)$_3$]$^+$, 318 [M-(CO)$_4$]$^+$, 290 [M-(CO)$_5$]$^+$, 262 [M-(CO)$_6$]$^+$; $\tilde{\nu}$ (CO) [cm^{-1}] = 2073, 2027, 1983, 1966.

2g[11]

^{1}H NMR (400 MHz, $CDCl_3$, 297 K, TMS) δ (ppm) = 7.23 – 7.07 (m, 2H, Ar-H), 6.73 – 6.57 (m, 2H, Ar-H); MS (EI): m/z = 392 $[M\text{-}(CO)]^+$, 364 $[M\text{-}(CO)_2]^+$, 336 $[M\text{-}(CO)_3]^+$, 308 $[M\text{-}(CO)_4]^+$, 280 $[M\text{-}(CO)_5]^+$, 252 $[M\text{-}(CO)_6]^+$; $\tilde{\nu}$ (CO) [cm^{-1}] = 2074, 2050, 2031, 2001, 1980, 1960.

2h[5]

^{1}H NMR (400 MHz, $CDCl_3$, 297 K, TMS) δ (ppm) = 7.92 – 6.80 (m, 10H, Ar-H); MS (EI): m/z = 498 $[M]^+$, 470 $[M\text{-}(CO)]^+$, 442 $[M\text{-}(CO)_2]^+$, 358 $[M\text{-}(CO)_5]^+$, 330 $[M\text{-}(CO)_6]^+$; $\tilde{\nu}$ (CO) [cm^{-1}] = 2068, 2033, 1993, 1985, 1976.

2i[12]

^{1}H NMR (400 MHz, $[D_2]$DCM, 297 K, TMS) δ (ppm) = 7.53 – 7.15 (m, 10H, Ar-H); ^{77}Se{^{1}H} NMR (76 MHz, $CDCl_3$, 297 K) δ (ppm) = 321.66, 280.64, 226.17; MS (EI): m/z = 594 $[M]^+$, 566 $[M\text{-}(CO)]^+$, 538 $[M\text{-}(CO)_2]^+$, 510 $[M\text{-}(CO)_3]^+$, 482 $[M\text{-}(CO)_4]^+$, 454 $[M\text{-}(CO)_5]^+$, 426 $[M\text{-}(CO)_6]^+$; $\tilde{\nu}$ (CO) [cm^{-1}] = 2062, 2024, 1997, 1969; elemental analysis calcd. (%) for $C_{18}H_{10}Fe_2O_6Se_2$: C 36.53, H 1.70; found: C 36.81, H 1.67.

2j[13]

^{1}H NMR (400 MHz, $[D_2]$DCM, 297 K, TMS) δ (ppm) = 7.52 – 7.37 (m, 2H, Ar-H), 7.35 – 7.24 (m, 4H, Ar-H), 7.24 – 7.16 (m, 2H, Ar-H), 7.16 – 7.07 (m, 2H, Ar-H); ^{125}Te{^{1}H} NMR (126 MHz, $[D_2]$DCM, 297 K) δ (ppm) = 485.10, 440.61; MS (EI): m/z = 689 $[M]^+$, 661 $[M\text{-}CO]^+$, 633 $[M\text{-}(CO)_2]^+$, 605 $[M\text{-}(CO)_3]^+$, 577 $[M\text{-}(CO)_4]^+$, 549 $[M\text{-}(CO)_5]^+$, 521 $[M\text{-}(CO)_6]^+$; $\tilde{\nu}$ (CO) [cm^{-1}] = 2050, 2009, 1993, 1970, 1941; elemental analysis calcd. (%) for $C_{18}H_{10}Fe_2O_6Te_2$: C 31.37, H 1.46; found: C 31.52, H 1.38.

2k[14]

^{1}H NMR (300 MHz, $CDCl_3$, 297 K, TMS) δ (ppm) = 7.06 (br s, 4H, Ar-H), 6.49 (br d, *J* = 6.9 Hz, 4H, Ar-H), 3.68 (br s, 4H, NH_2); MS (EI): m/z = 528 $[M]^+$, 499 $[M\text{-}(CO)H]^+$, 471 $[M\text{-}(CO)_2H]^+$, 444 $[M\text{-}(CO)_3]^+$, 388 $[M\text{-}(CO)_5]^+$, 360 $[M\text{-}(CO)_6]^+$; $\tilde{\nu}$ (CO) [cm^{-1}] = 2070, 2064, 2026, 1992, 1982, 1973, 1961.

2l[15]

^{1}H NMR (400 MHz, $CDCl_3$, 297 K, TMS) δ (ppm) = 7.87 (d, *J* = 7.0 Hz, 2H, Ar-H), 7.64 (d, J = 7.0 Hz, 2H, Ar-H), 7.36 (m, 4H, Ar-H), 2.76 (s, 4H, CH_2); MS (EI): m/z = 536 [M]+, 508 [M-CO]+, 480 [M-(CO)2]+, 452 [M-(CO)3]+, 424 [M-(CO)4]+, 396 $[M\text{-}(CO)_5]^+$, 368 $[M\text{-}(CO)_6]^+$; $\tilde{\nu}$ (CO) [cm^{-1}] = 2068, 2019, 2003, 1962.

2m[16]

^{1}H NMR (400 MHz, $[D_8]$THF, 297 K, TMS) δ (ppm) = 8.55 - 8.49 (d, $^3J_{H\text{-}H}$ = 7.6 Hz, 2H; Ar-NMI), 8.43 (d, $^3J_{H\text{-}H}$ = 7.6 Hz, 2H; Ar-NMI), 4.84 (d, $^4J_{H\text{-}H}$ = 2.4 Hz, 2H; CH_2), 2.54 (t, $^4J_{H\text{-}H}$ = 2.4 Hz, 1H; CC*H*); MS (EI): m/z = 577 $[M]^+$, 549 $[M\text{-}CO]^+$, 521 $[M\text{-}(CO)_2]^+$, 493 $[M\text{-}(CO)_3]^+$, 465 $[M\text{-}(CO)_4]^+$, 437 $[M\text{-}(CO)_5]^+$, 409 $[M\text{-}(CO)_6]^+$; $\tilde{\nu}$ (CO) [cm^{-1}] = 2073, 2049, 2029, 2008, 1997, 1984, 1979, 1975; elemental analysis calcd. (%) for $C_{21}H_7Fe_2NO_8S_2$: C 43.71, H 1.22, N 2.43, S 11.11; found: C 43.91, H 1.32, N 2.41, S 10.98.

2n[17]

^{1}H NMR (400 MHz, $CDCl_3$, 297 K, TMS) δ (ppm) = 8.49 – 8.42 (m, 4H, Ar-Ph), 7.35 (d, $^3J_{H\text{-}H}$ = 8.2 Hz, 2H, Ar-NMI), 7.17 (d, $^3J_{H\text{-}H}$ = 8.2 Hz, 2H, Ar-NMI), 2.45 (s, 3H, CH_3); MS (EI): m/z = 629 $[M]^+$, 601 $[M\text{-}CO]^+$, 573 $[M\text{-}(CO)_2]^+$, 516 $[M\text{-}(CO)_4H]^+$, 488 $[M\text{-}(CO)_5H]^+$; $\tilde{\nu}$ (CO) [cm^{-1}] = 2080, 2039, 2008, 1986, 1963.

$Fe_3(CO)_{11}$NMP

In a Schlenk flask **$Fe_3(CO)_{12}$** (939 mg, 1.87 mmol) was dissolved in anhydrous, N_2-saturated toluene/NMP mixture (10:1, 11 mL) and heated at 50 °C for 5 minutes, until the dark green solution turned purple, monitored by TLC. After complete consumption of the starting material, the solution was cooled down to RT. The target compound could be isolated as a purple, oxygen-sensitive solid after purification via column chromatography (*n*-hexane/acetone (1:0 -> 1:1)).

^{1}H NMR (400 MHz, benzene-d6, 297 K, TMS) δ (ppm) = 2.54 – 2.38 (m, 5H), 2.00 (br t, $^3J_{H\text{-}H}$ = 8.2 Hz, 2H), 1.21 (quin, $^3J_{H\text{-}H}$ = 7.6 Hz, 2H); ^{13}C{^{1}H} NMR (101 MHz, benzene-d6, 297 K, TMS) δ (ppm) = 174.76, 49.01, 30.89, 29.50, 17.77; MS (ESI negative mode): m/z = 573.7 $[M\text{-}H]^-$ (calc. 573.8), 545.7 $[M\text{-}H(CO)]^-$ (calc. 545.8), IR (toluene, 297 K) $\tilde{\nu}$ (cm^{-1}) = 2018, 1996.

NMP

^{1}H NMR (400 MHz, benzene-d6, 297 K, TMS) δ (ppm) = 2.54 – 2.43 (m, 5H), 1.94 (t, J = 8.1 Hz, 2H), 1.32 – 1.10 (m, 2H); ^{13}C{^{1}H} NMR (101 MHz, benzene-d6, 297 K, TMS) δ (ppm) = 173.86, 48.76, 30.72, 29.41, 17.91.

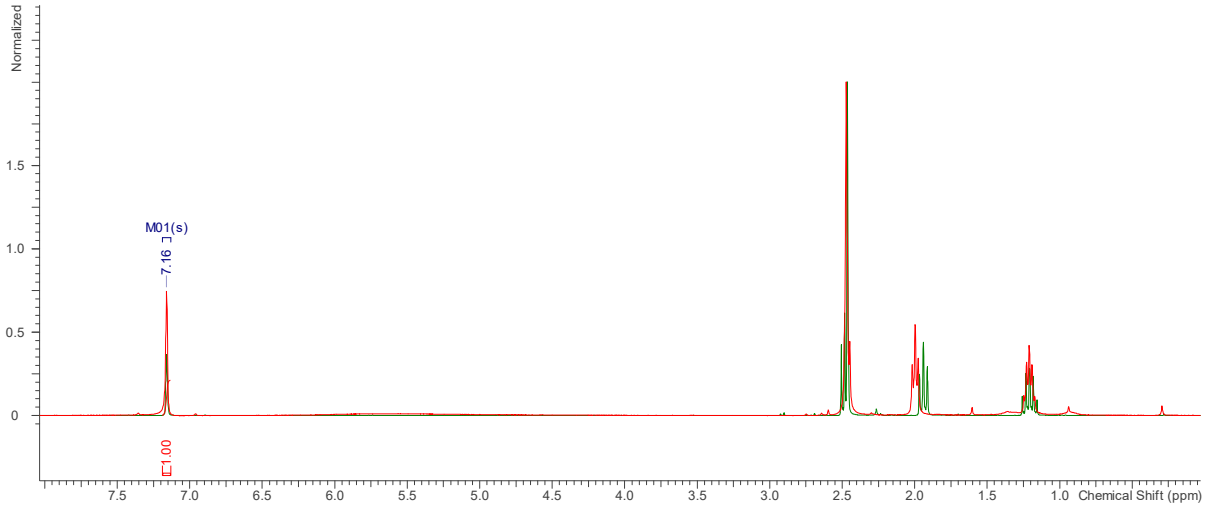

Figure S4. ^{1}H NMR (benzene-d$_6$, 400 MHz, 298 K) of Fe$_3$(CO)$_{11}$NMP (red) and NMP (green)

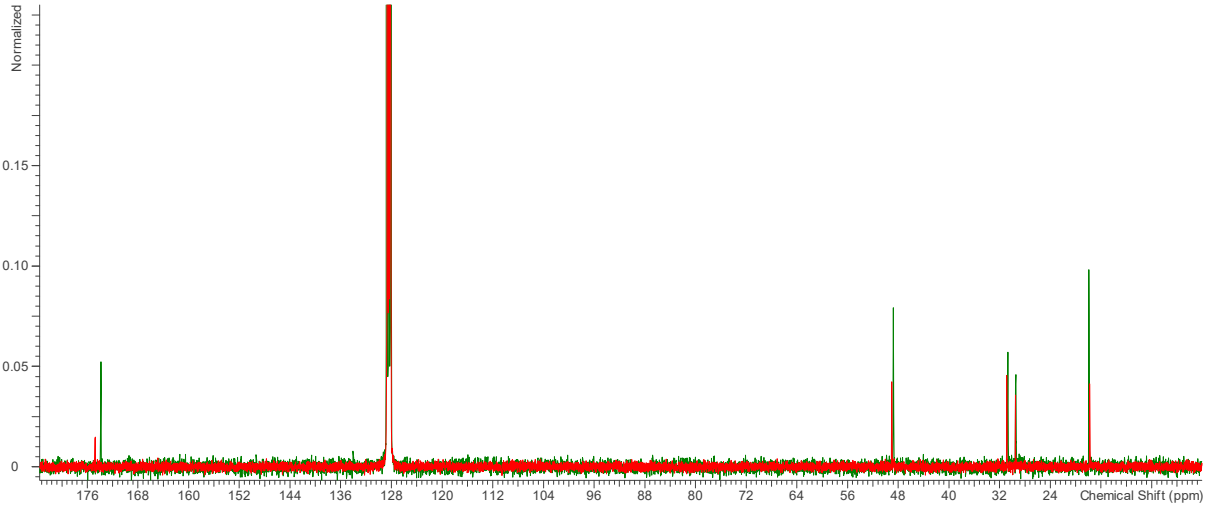

Figure S5. ^{13}C{^{1}H} NMR (benzene-d$_6$, 100 MHz, 298 K) of Fe$_3$(CO)$_{11}$NMP (red) and NMP (green)

Proton NMR spectra (Figure S4) show small downfield shift around 2.0 ppm and 2.5 ppm, indicating the coordination of NMP to the triiron cluster with a small loss of electron density, as expected. A similar behavior was observed in the carbon NMR spectra, revealed by the small downfield shift of the carbonyl carbon of the NMP at 174 ppm.

Quantum chemistry

Quantum chemical calculations determining structural and electronic properties of **Fe$_3$(CO)$_{11}$NMP** were performed using Gaussian 16.[18] Fully relaxed singlet ground state equilibrium geometries were obtained for three preselected isomers of **Fe$_3$(CO)$_{11}$NMP**, which are denoted **A**, **B** and **C** (see Figure S14). To this aim, density functional theory (DFT) was applied using the B3LYP XC functional,[19] while the def2-SVP basis set was applied for all atoms.[20] Subsequently, a vibrational analysis was carried out to verify that a minimum on the 3N-6 potential energy (hyper)surface (PES) was obtained for each redox species. To correct for the lack of anharmonicity and the approximate treatment of electron correlation, the harmonic frequencies were scaled by the factor 0.97.[21]

Furthermore, excited state properties such as excitation energies, oscillator strengths and electronic characters for the lowest 50 excited states were calculated within the equilibrium structures of the respective isomer, i.e. **A**, **B** and **C**, at the time-dependent DFT (TDDFT) level of theory. Therefore, the same computational protocol was applied as in case for the preceding DFT simulations. Several computational as well as joint spectroscopic-theoretical studies on structurally related [FeFe] H$_2$ase mimics showed that this computational protocol enables an accurate prediction of ground and excited states properties with respect to experimental data, e.g. structural and electrochemical properties as well as with respect to UV-Vis absorption.[16,22] Effects of interaction with a solvent (toluene: ε = 2.3741, n = 1.4969) were taken into account on the ground and excited states properties by the solute electron density (SMD) variant of the integral equation formalism of the polarizable continuum model.[23] All calculations were performed including D3 dispersion correction with Becke-Johnson damping.[24]

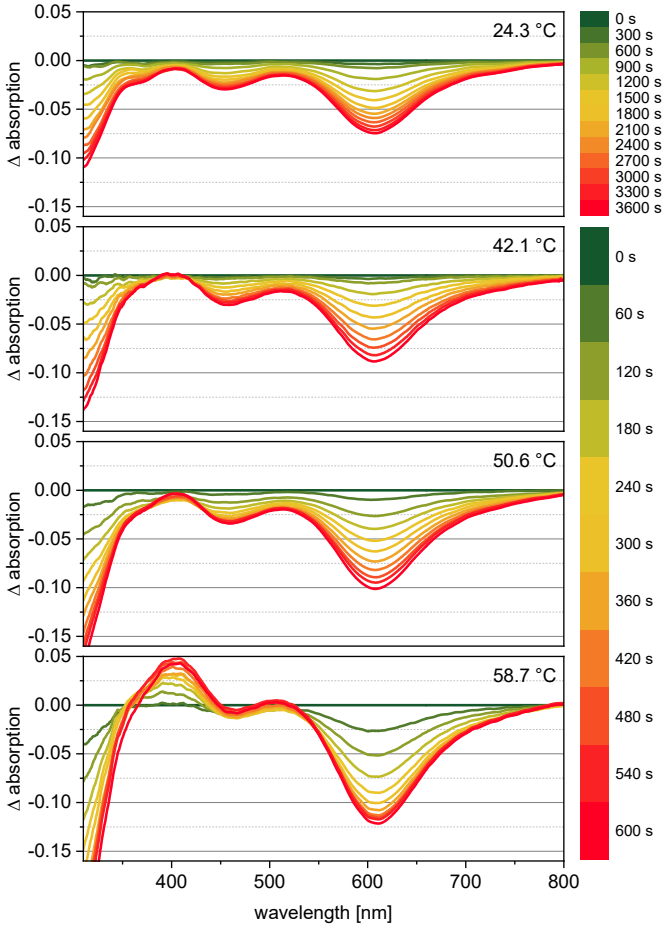

Figure S6. Differential UV-Vis spectra during the reaction of 1,3-propane-dithiol (1a) with equimolar amounts of $Fe_3(CO)_{12}$ (toluene/NMP (10:1), c = 2.2 x 10^{-4} M) at varying temperatures. The Δ absorbance spectra were calculated by subtracting the first spectrum (0 s).

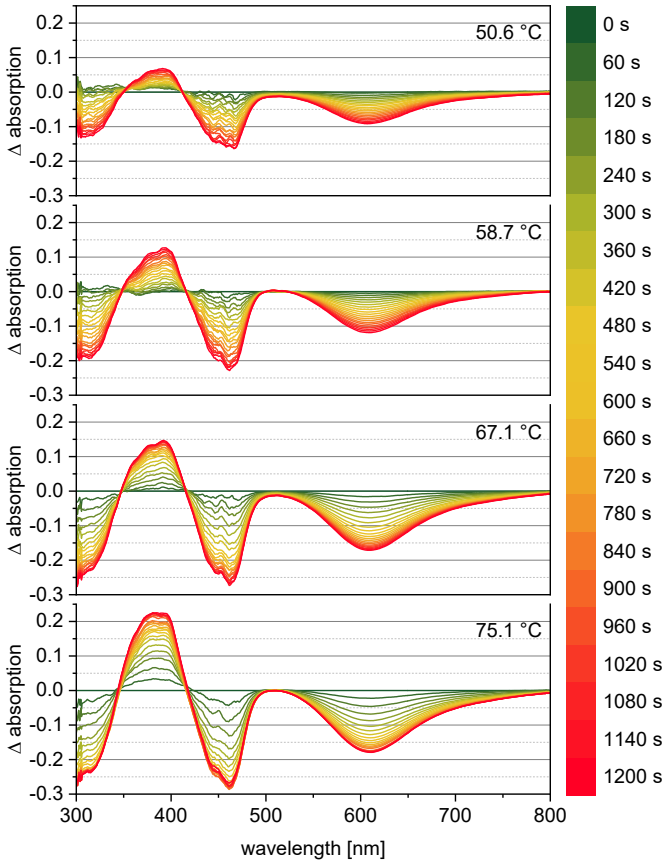

Figure S7. Differential UV-Vis spectra during the reaction of 1n with equimolar amounts of $Fe_3(CO)_{12}$ (toluene/NMP (10:1), c = 2.2 x 10^{-4} M) at varying temperatures. The Δ absorbance spectra were calculated by subtracting the first spectrum (0 s).

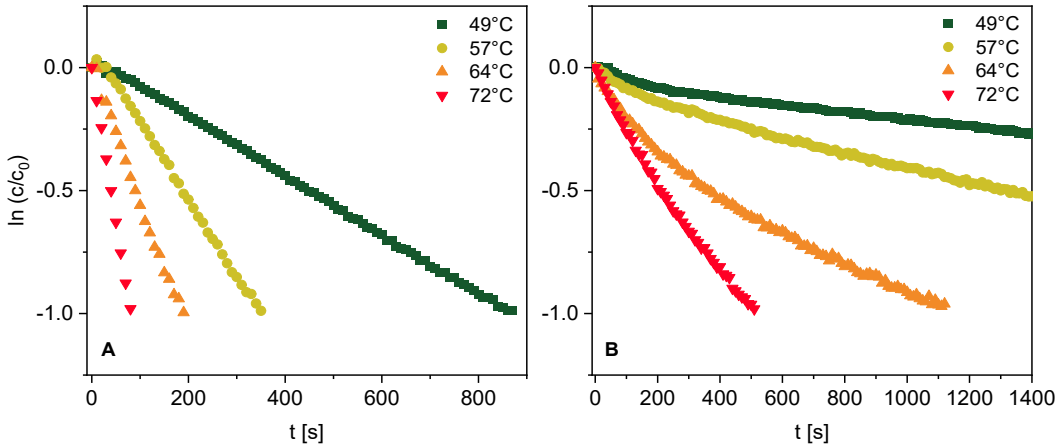

Figure S8. Plots of the natural logarithm of the relative concentration of $Fe_3(CO)_{12}$ versus time at varying temperatures during the reaction with excess amount of 1n in presence (A) and absence (B) of NMP, respectively.

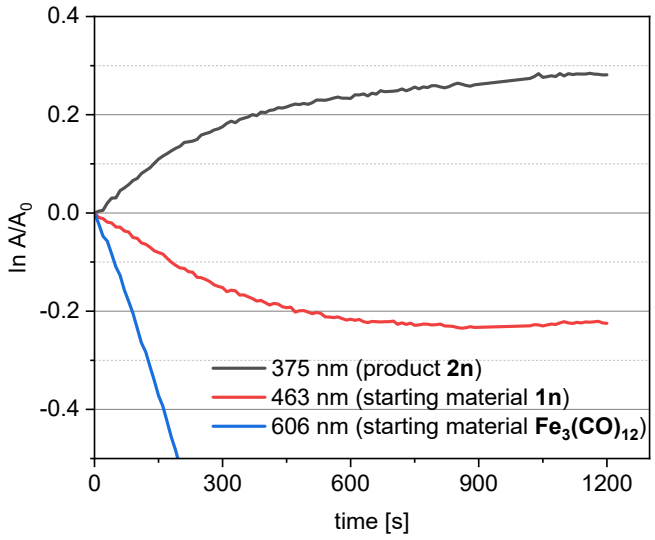

Figure S9. Plot of ln A/A_0 vs time during the reaction of 1n with equimolar amounts of $Fe_3(CO)_{12}$ (c = 2.2 x 10^{-4} M) at 75.1 °C.

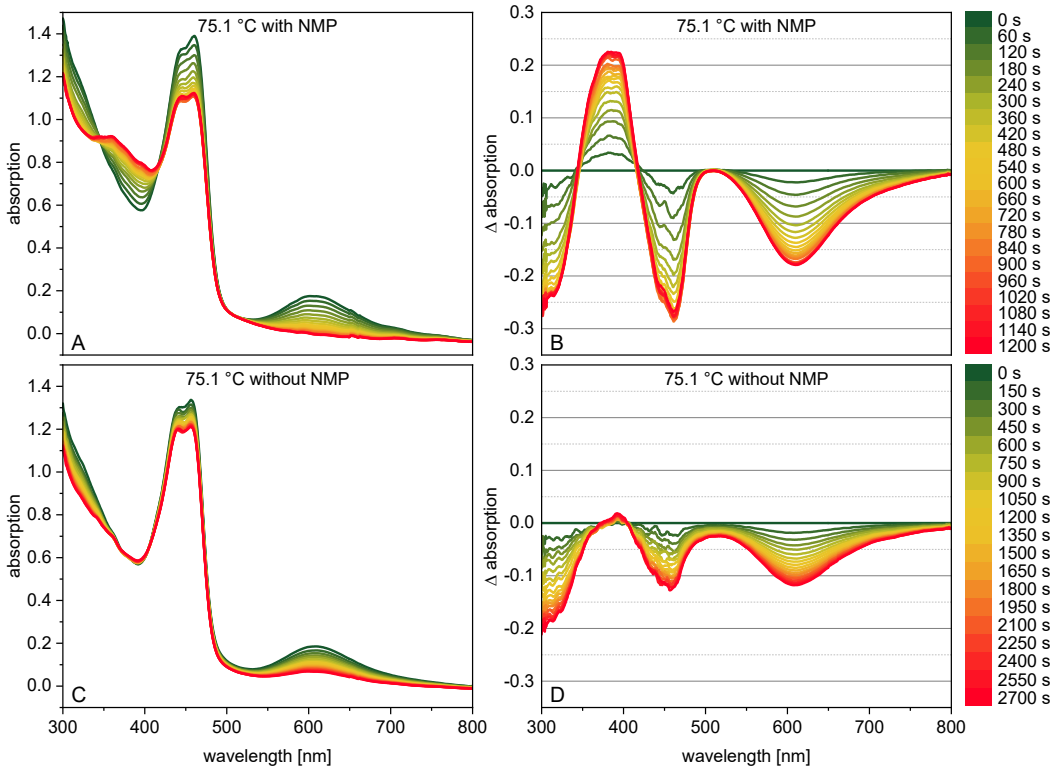

Figure S10. UV-Vis spectra (A, C) and differential UV-Vis spectra (B, D) during the reaction of 1n with equimolar amounts of $Fe_3(CO)_{12}$ (c = 2.2 x 10^{-4} M) with and without NMP at 75.1 °C. The Δ absorbance spectra were calculated by subtracting the first spectrum (0 s).

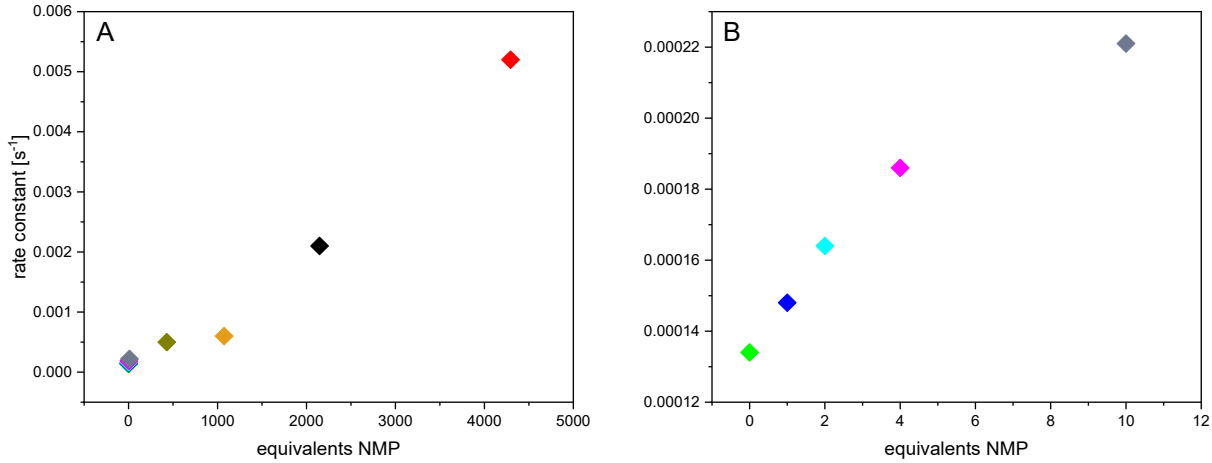

Figure S11. Rate constant dependency towards the concentration of added NMP for the reaction of 1a with equimolar amounts of $Fe_3(CO)_{12}$ (toluene, *c* = 2.2 x 10^{-4} M) at 50.85 °C. Figure B shows the zoomed area of low equivalents.

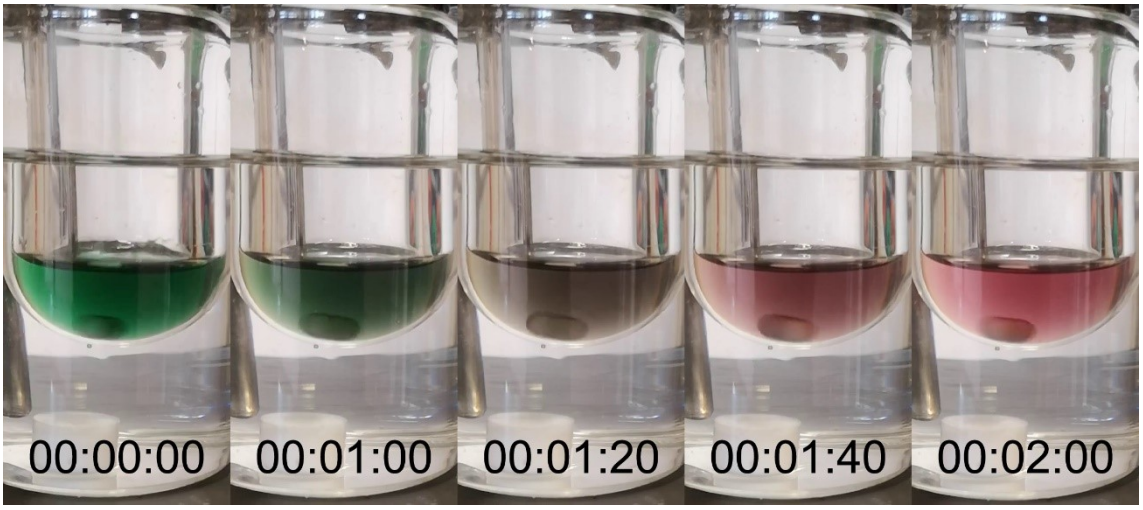

Figure S12. Photographs during the reaction of $Fe_3(CO)_{12}$ with NMP (toluene/NMP (10:1), *c* ≈ 2.2 x 10^{-3} M) at 52 °C.

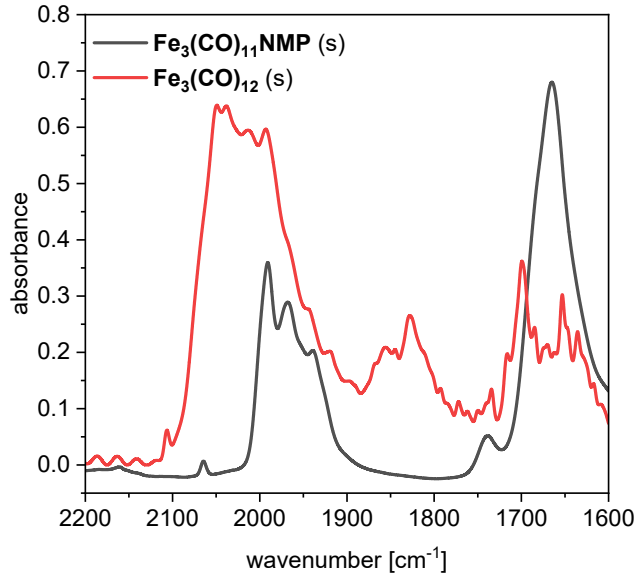

Figure S13. IR spectra of $Fe_3(CO)_{12}$ and its NMP-substituted analogue in solid state.

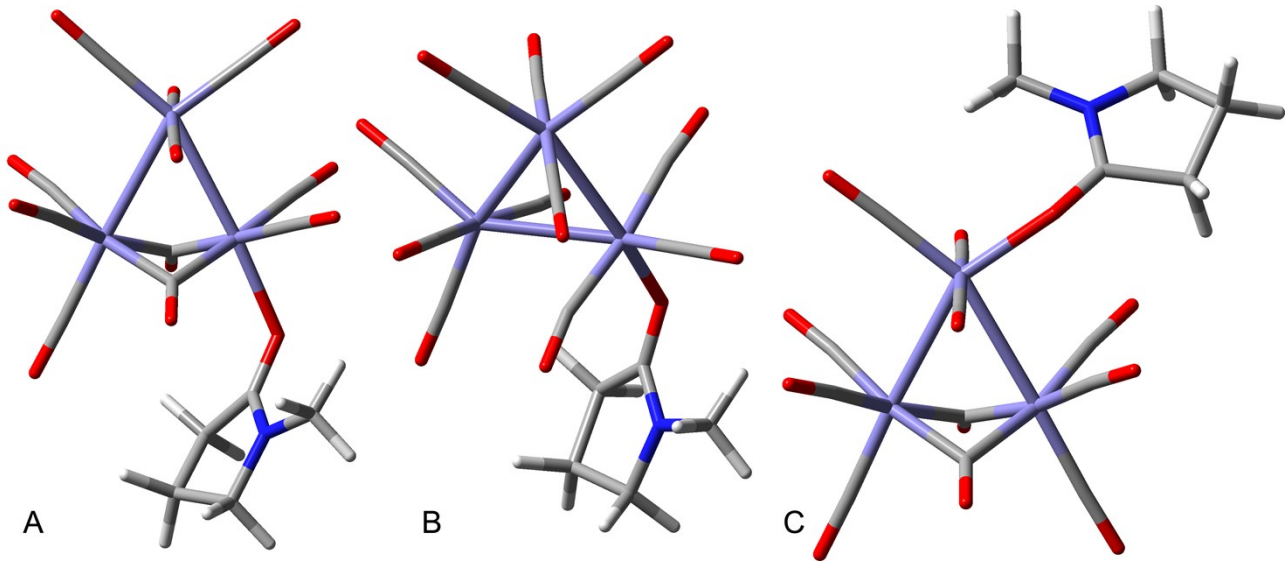

Figure S14. Simulated isomeric structures of $Fe_3(CO)_{11}$NMP.

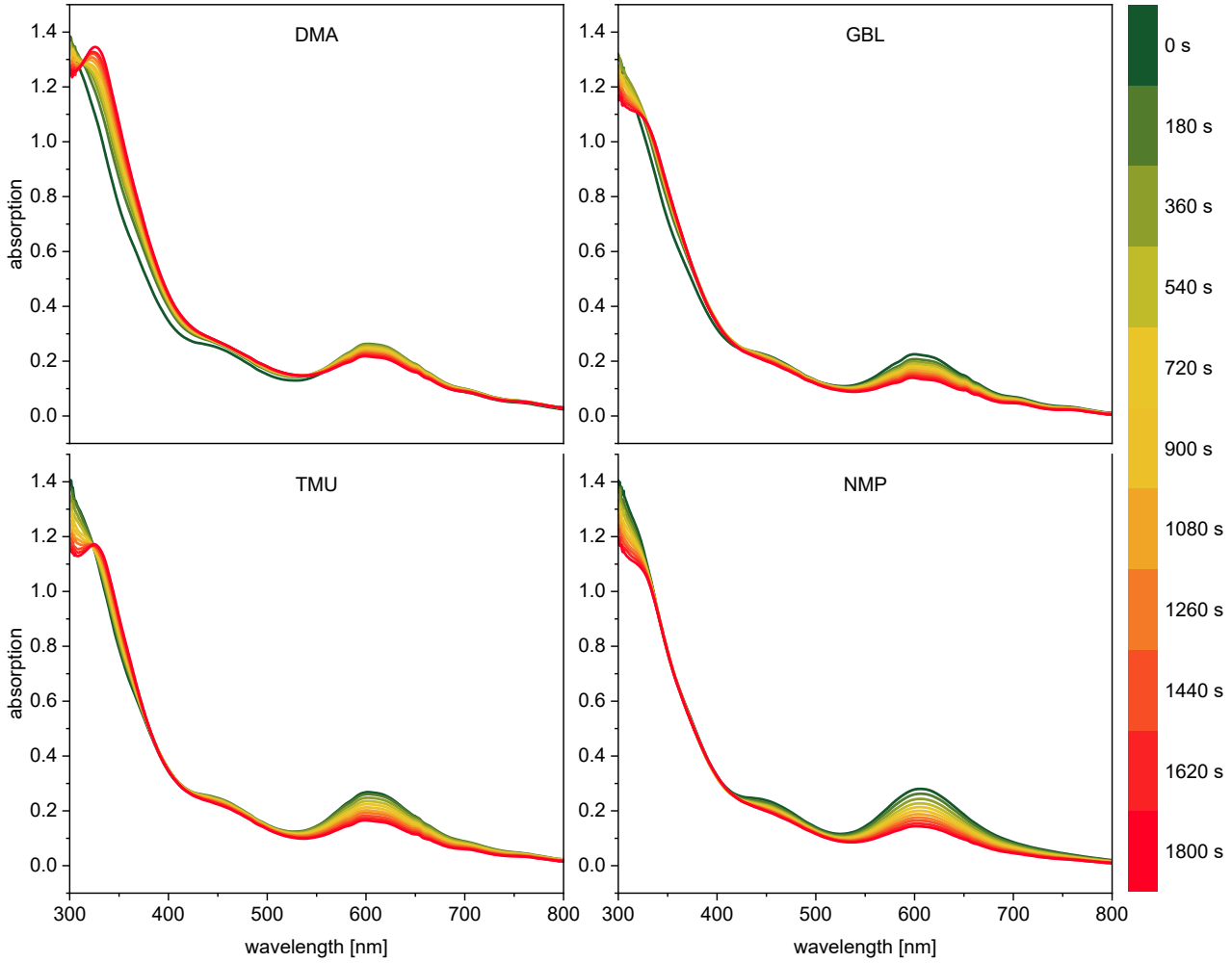

Figure S15. UV-Vis spectra during the reaction of 1a with $Fe_3(CO)_{12}$ (toluene/additive (10:1), c = 2.2 x 10^{-4} M, T = 42 °C) with varying additives.

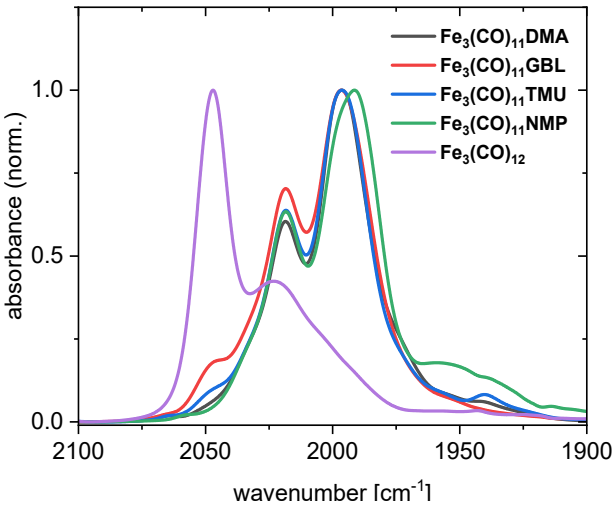

Figure S16. Normalized IR spectra of the substitution products of $Fe_3(CO)_{12}$ with dimethylacetamide (DMA), γ-butyrolactone (GBL), tetramethylurea (TMU) and *N*-methylpyrrolidone (NMP) as well as their starting material $Fe_3(CO)_{12}$.

Table S1: Electronic properties, such as excitation energies (*E*), wavelengths (*λ*), oscillator strengths (*f*) and electronic nature (ligand field, LF), of dipole-allowed transitions contributing to the UV-Vis absorption spectra of the three isomers of $Fe_3(CO)_{11}NMP$.

A (ΔG = 14.2 kJ mol^{-1})				
State	Character	*E* / eV	λ / nm	*f*
S_1	LF	1.63	762	0.0031
S_2	LF	1.70	730	0.0117
S_4	LF	2.43	511	0.0239
S_6	LF	2.61	474	0.0317
S_7	LF	2.71	457	0.0207
S_{11}	LF	3.01	412	0.0204
B (ΔG = 0.0 kJ mol^{-1})				
State	Character	*E* / eV	λ / nm	*f*
S_1	LF	1.64	755	0.0168
S_2	LF	1.88	659	0.0136
S_3	LF	2.08	596	0.0145
S_4	LF	2.38	522	0.0091
S_5	LF	2.47	501	0.0045
S_6	LF	2.57	483	0.0284
C (ΔG = 15.1 kJ mol^{-1})				
State	Character	*E* / eV	λ / nm	*f*
S_1	LF	1.74	712	0.0062
S_2	LF	1.76	704	0.0136
S_3	LF	2.23	557	0.0525
S_5	LF	2.57	482	0.0187
S_{11}	LF	3.05	407	0.0169

Table S2: Electronic character of dipole-allowed transitions contributing to the UV-Vis absorption spectra of the three isomers of $Fe_3(CO)_{11}NMP$ as visualized by charge density differences; charge transfer occurs from red to blue.

A (ΔG = 14.2 kJ mol^{-1})

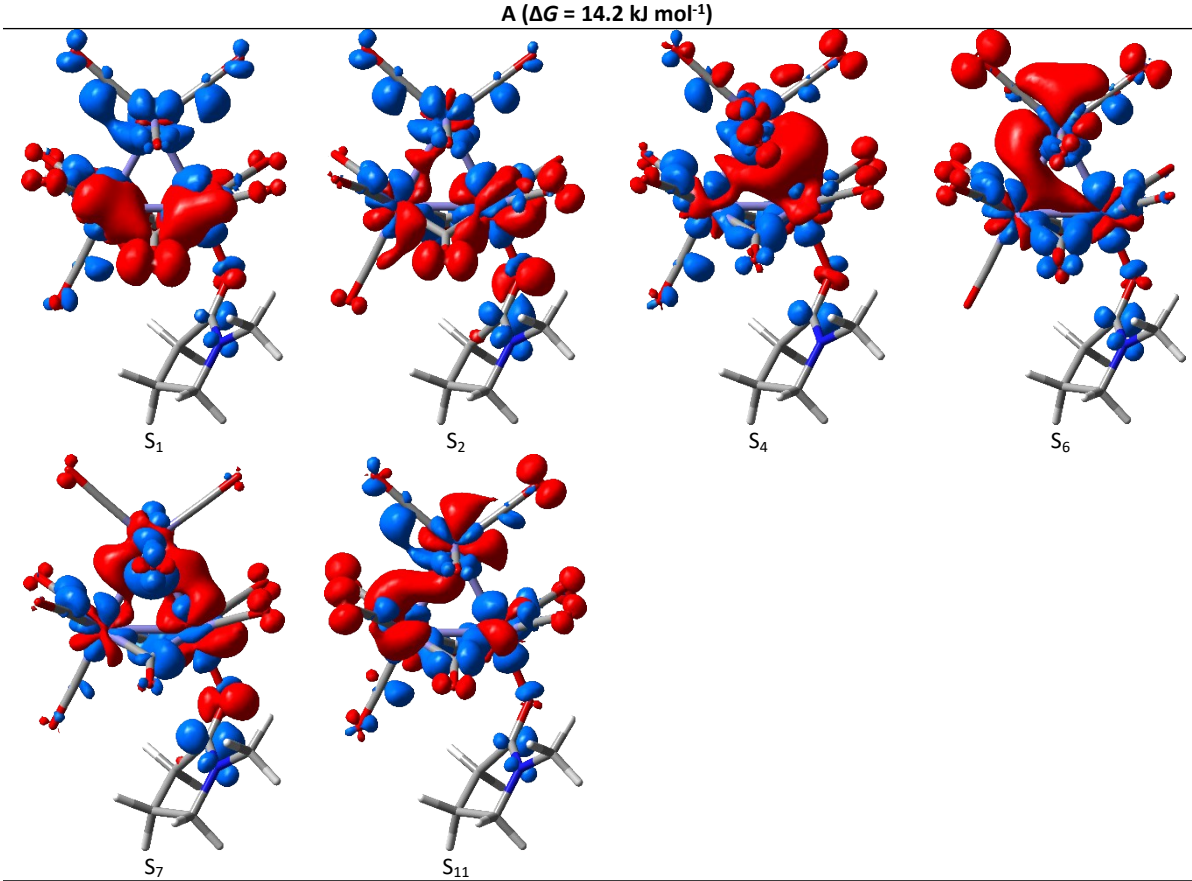

B (ΔG = 0.0 kJ mol^{-1})

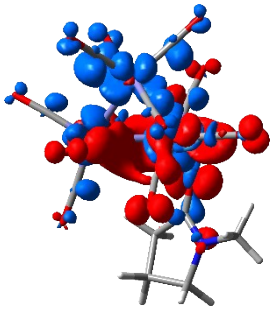

S_1

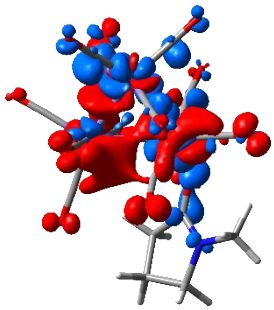

S_2

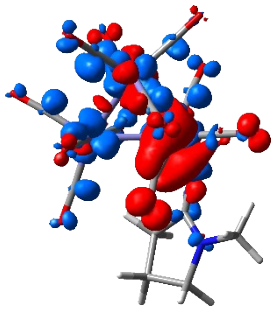

S_3

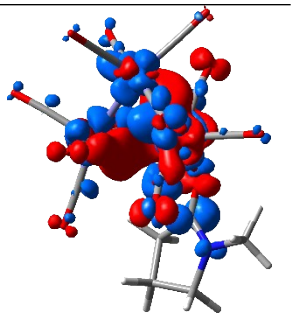

S_4

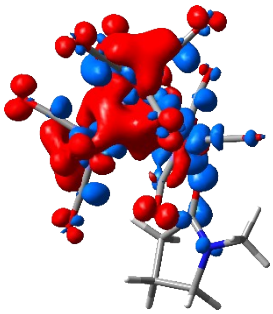

S_5

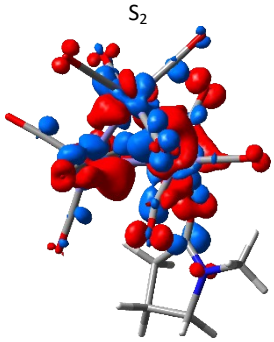

S_6

C (ΔG = 15.1 kJ mol^{-1})

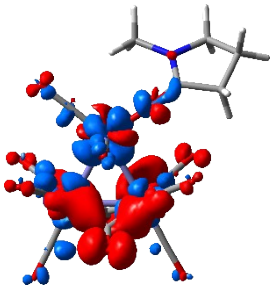

S_1

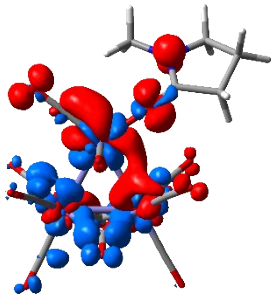

S_2

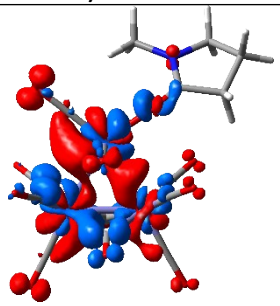

S_3

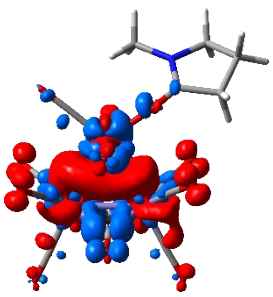

S_5

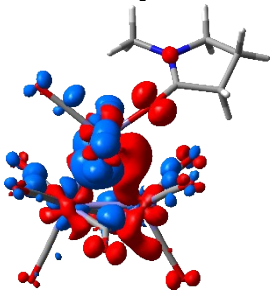

S_{11}

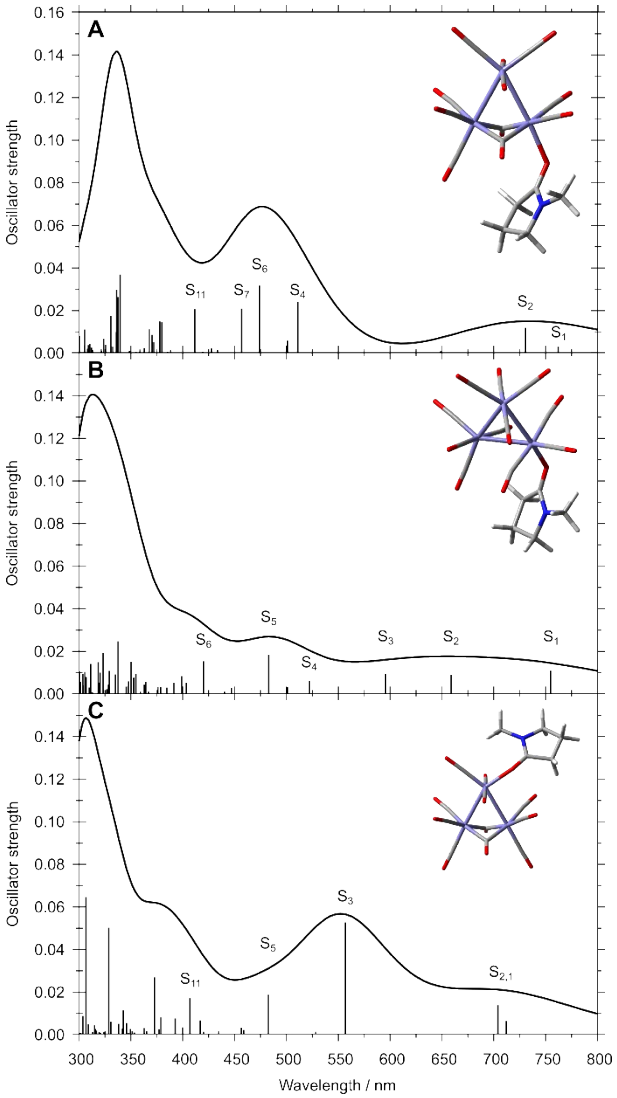

Figure S17. Simulated UV-Vis absorption spectra of the three isomers of $Fe_3(CO)_{11}$NMP, i.e., A, B and C. Prominent electronic transitions are labeled.

Table S3: Simulated vibrational normal modes of $Fe_3(CO)_{11}$NMP associated to CO-stretching, i.e. to the carbonyl group of NMP (mode 97), to the bridging CO ligands (modes 98 and 99) and to the terminal CO ligands (modes 100-108). Predicted frequencies ($\tilde{\upsilon}_{CO}$; unscaled and scaled by a factor of 0.97)[21,25] and IR intensities (I_{IR}) are given for the three isomers, i.e., A, B and C.

	A (ΔG = 14.2 kJ mol^{-1})			B (ΔG = 0.0 kJ mol^{-1})			C (ΔG = 15.1 kJ mol^{-1})		
Mode	$\tilde{\upsilon}_{CO}$ / cm^{-1}	$\tilde{\upsilon}^{scaled}_{CO}$ / cm^{-1}	I_{IR} / km mol^{-1}	$\tilde{\upsilon}_{CO}$ / cm^{-1}	$\tilde{\upsilon}^{scaled}_{CO}$ / cm^{-1}	I_{IR} / km mol^{-1}	$\tilde{\upsilon}_{CO}$ / cm^{-1}	$\tilde{\upsilon}^{scaled}_{CO}$ / cm^{-1}	I_{IR} / km mol^{-1}
97 (CO_{NMP})	1681	1631	1144	1680	1629	1206	1707	1656	1427
98 ($CO_{\mu2}$)	1868	1812	967	1978	1918	389	1894	1837	1054
99 ($CO_{\mu2}$)	1924	1867	656	1994	1934	476	1932	1874	532
100 (CO)	2030	1969	124	2016	1955	24	2010	1950	122
101 (CO)	2033	1972	514	2023	1962	414	2027	1966	679
102 (CO)	2042	1981	111	2030	1969	431	2035	1974	808
103 (CO)	2048	1987	688	2037	1976	1501	2041	1980	300
104 (CO)	2050	1988	141	2047	1986	575	2051	1989	205
105 (CO)	2061	2000	2673	2051	1990	2237	2058	1997	2367
106 (CO)	2064	2002	1854	2066	2004	2029	2070	2008	2649
107 (CO)	2074	2012	3592	2069	2007	3523	2077	2015	2785
108 (CO)	2147	2082	270	2145	2080	216	2145	2081	105

Table S4: Vibrational normal modes of three isomers of $Fe_3(CO)_{11}$NMP associated to CO-stretching, i.e. to the carbonyl group of NMP (mode 97), to the bridging CO ligands (modes 98 and 99) and to the terminal CO ligands (modes 100-108) as visualized by displacement vectors.

A (ΔG = 14.2 kJ mol^{-1})			
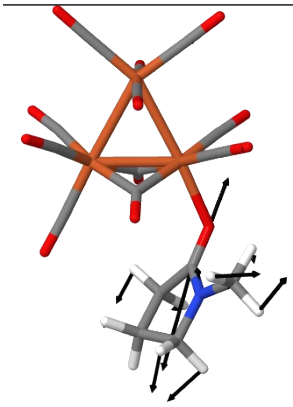 97 (CO_{NMP})	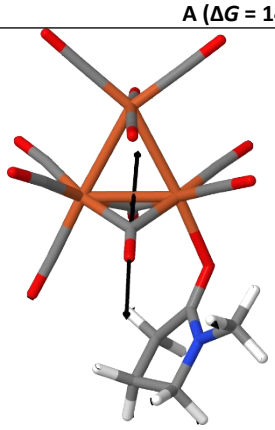 98 ($CO_{\mu 2}$)	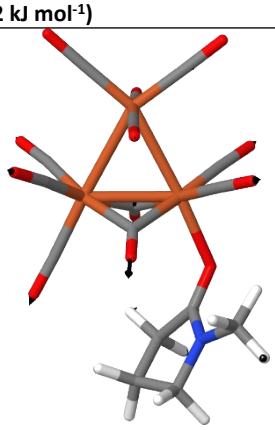 99 ($CO_{\mu 2}$)	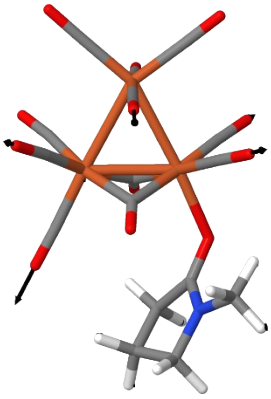 100 (CO)
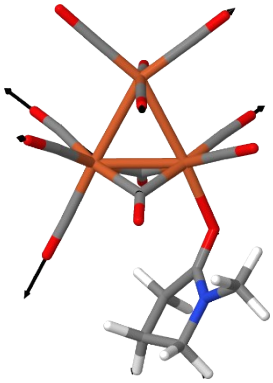 101 (CO)	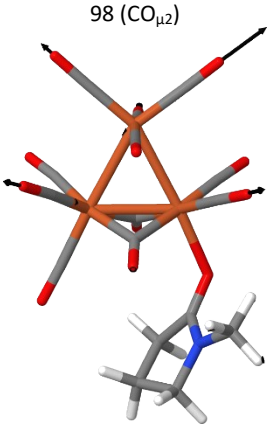 102 (CO)	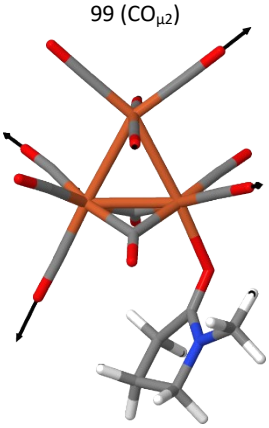 103 (CO)	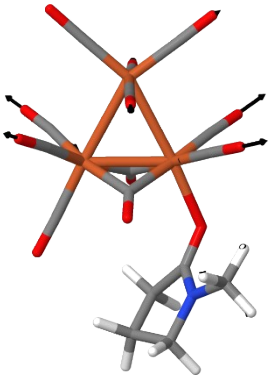 104 (CO)
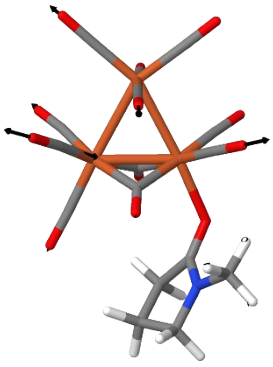 105 (CO)	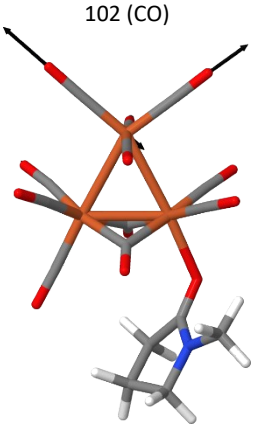 106 (CO)	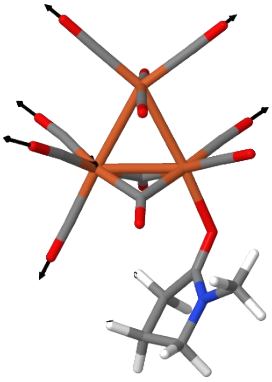 107 (CO)	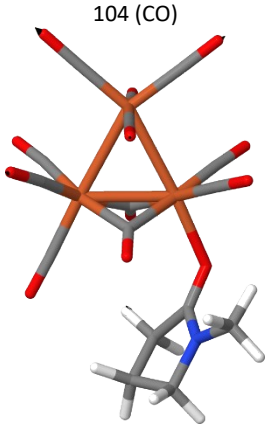 108 (CO)
B (ΔG = 0.0 kJ mol^{-1})			
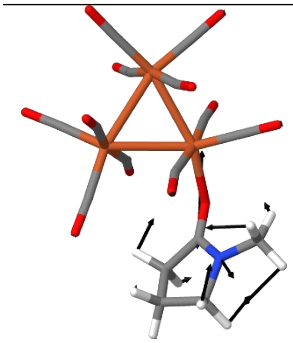 97 (CO_{NMP})	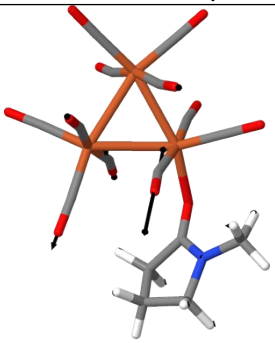 98 ($CO_{\mu 2}$)	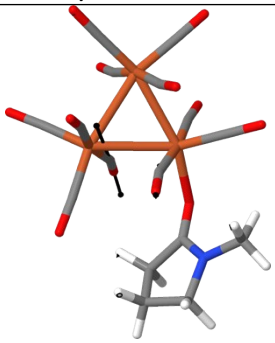 99 ($CO_{\mu 2}$)	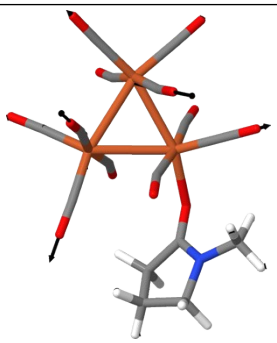 100 (CO)

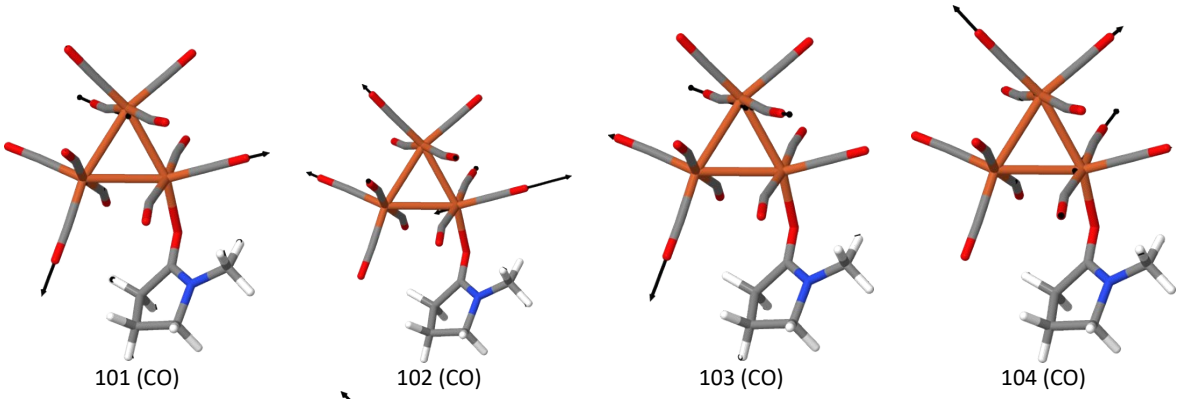

101 (CO) 102 (CO) 103 (CO) 104 (CO)

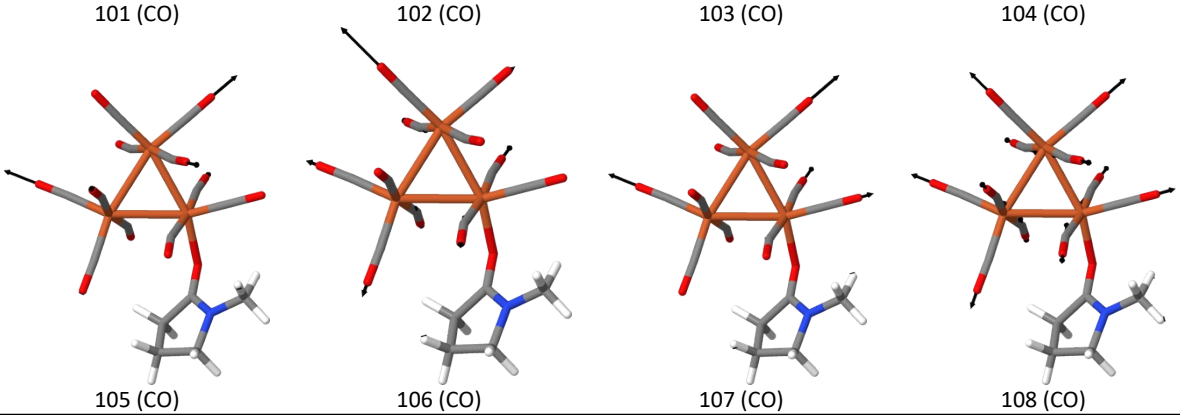

105 (CO) 106 (CO) 107 (CO) 108 (CO)

C (ΔG = 15.1 kJ mol^{-1})

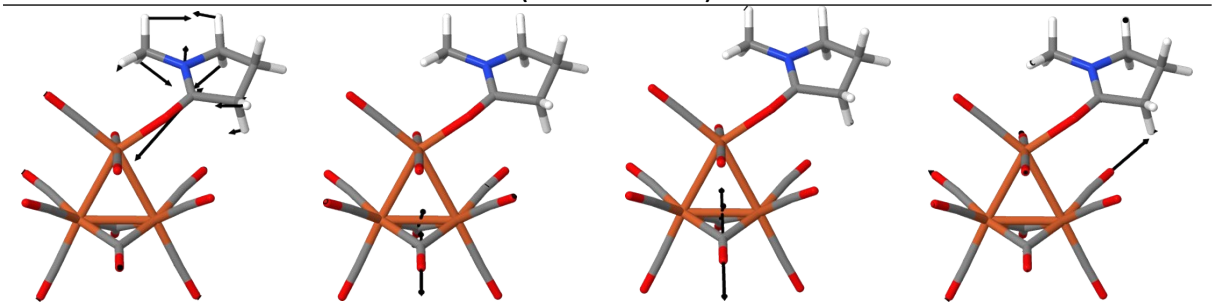

97 (CO_{NMP}) 98 ($CO_{\mu2}$) 99 ($CO_{\mu2}$) 100 (CO)

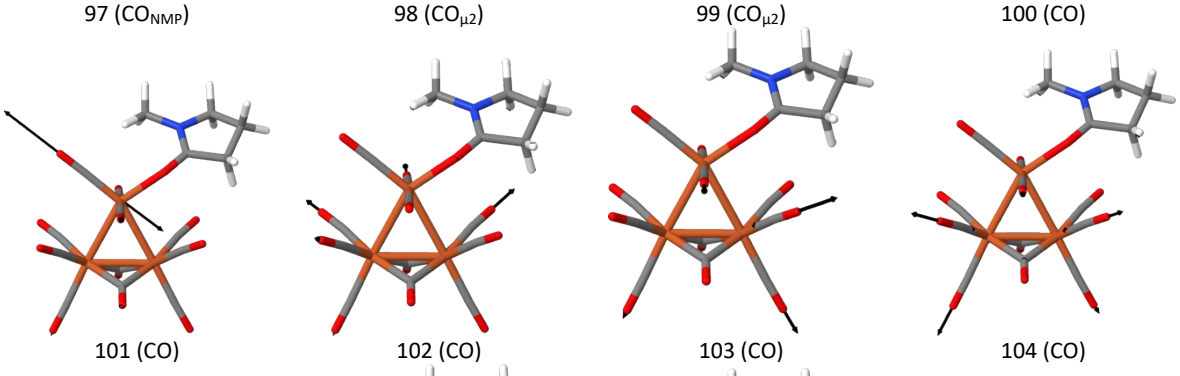

101 (CO) 102 (CO) 103 (CO) 104 (CO)

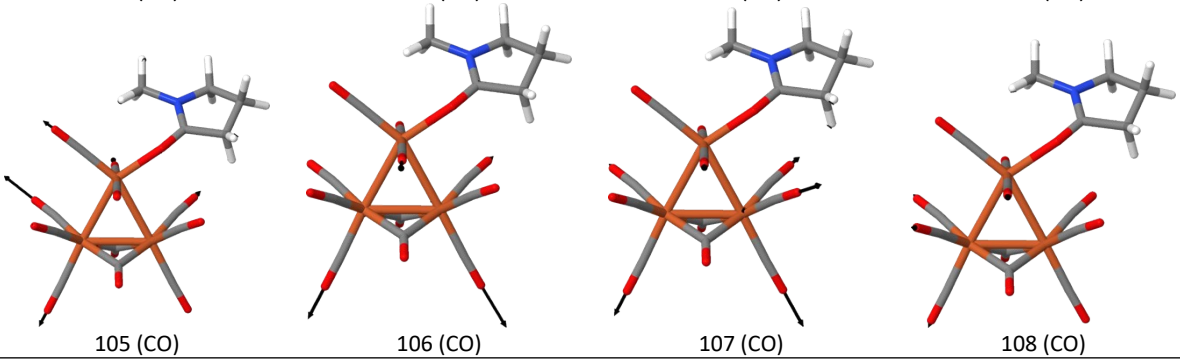

105 (CO) 106 (CO) 107 (CO) 108 (CO)

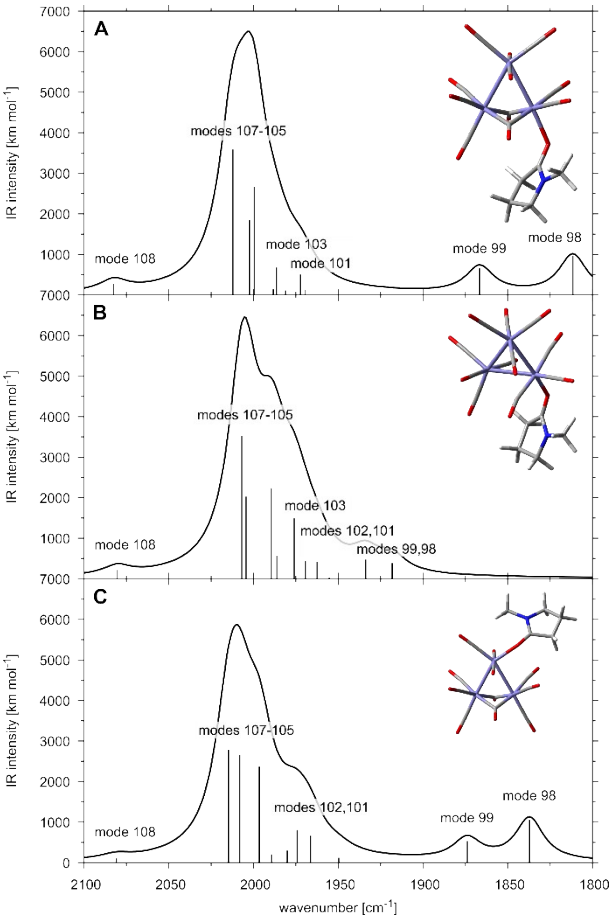

Figure S18. Simulated IR spectra of the three isomers of $Fe_3(CO)_{11}NMP$, i.e., A, B and C. Prominent vibrational modes are labeled.

References

1 a) COLLECT Data Collection Software and Nonius B.V., Netherlands, 1998; b) Z. Otwinowski, Minor, W. in Carter, C. W. and Sweet, R. M. (eds.), *Processing of X-Ray Diffraction Data Collected in Oscillation Mode. Methods in Enzymology, Vol. 276, Macromolecular Crystallography, Part A*, Academic Press, 1997, 307; c) Bruker-AXS inc., *SADABS 2.10*, Madison, WI, U.S.A, 2002;

2 G. M. Sheldrick, *Acta Crystallogr., Sect. A: Found. Crystallogr.*, 2015, **71**, 3.

3 G. M. Sheldrick, *Acta Crystallogr. Sect. C: Struct Chem*, 2015, **71**, 3.

4 C. F. Macrae, P. R. Edgington, P. McCabe, E. Pidcock, G. P. Shields, R. Taylor, M. Towler and J. van de Streek, *J. Appl. Crystallogr.*, 2006, **39**, 453.

5 Y. Si, M. Hu and C. Chen, *C.R. Chim.*, 2008, **11**, 932.

6 a) A. L. Haley, L. N. Broadbent, L. S. McDaniel, S. T. Heckman, C. H. Hinkle, N. N. Gerasimchuk, J. C. Hershberger and C. A. Mebi, *Polyhedron*, 2016, **114**, 218; b) H. T. Poh, B. T. Sim, T. S. Chwee, W. K. Leong and W. Y. Fan, *Organometallics*, 2014, **33**, 959;

7 X. Jiang, L. Long, H. Wang, L. Chen and X. Liu, *Dalton Trans.*, 2014, **43**, 9968.

8 U.-P. Apfel, Y. Halpin, H. Görls, J. G. Vos, B. Schweizer, G. Linti and W. Weigand, *C&B*, 2007, **4**, 2138.

9 L. Song, Q. Hu, Q. Dong and J. Wang, *Chin. J. Inorg. Chem.*, 1990, **6**, 256.

10 P. I. Volkers, T. B. Rauchfuss and S. R. Wilson, *Eur. J. Inorg. Chem.*, 2006, 4793.

11 L. Schwartz, P. S. Singh, L. Eriksson, R. Lomoth and S. Ott, *C.R. Chim.*, 2008, **11**, 875.

12 E. D. Schermer and W. H. Baddley, *J. Organomet. Chem.*, 1971, **30**, 67.

13 S. Lü, S. Gong, G.-H. Xu, Y.-Y. Liu, L. Lü, C.-R. Qin and Q.-L. Li, *Inorg. Chim. Acta*, 2020, **511**, 119797.

14 F. Wen, X. Wang, L. Huang, G. Ma, J. Yang and C. Li, *ChemSusChem*, 2012, **5**, 849.

15 R. Goy, L. Bertini, H. Görls, L. de Gioia, J. Talarmin, G. Zampella, P. Schollhammer and W. Weigand, *Chem. Eur. J.*, 2015, **21**, 5061.

16 S. Benndorf, E. Hofmeister, M. Wächtler, H. Görls, P. Liebing, K. Peneva, S. Gräfe, S. Kupfer, B. Dietzek-Ivanšić and W. Weigand, *Eur. J. Inorg. Chem.*, 2022, **3**, e202100959.

17 A. P. S. Samuel, D. T. Co, C. L. Stern and M. R. Wasielewski, *J. Am. Chem. Soc.*, 2010, **132**, 8813.

18 M. J. Frisch, G. W. Trucks, H. B. Schlegel, G. E. Scuseria, M. A. Robb, J. R. Cheeseman, G. Scalmani, V. Barone, G. A. Petersson, H. Nakatsuji, X. Li, M. Caricato, A. V. Marenich, J. Bloino, B. G. Janesko, R. Gomperts, B. Mennucci, H. P. Hratchian, J. V. Ortiz, A. F. Izmaylov, J. L. Sonnenberg, Williams, F. Ding, F. Lipparini, F. Egidi, J. Goings, B. Peng, A. Petrone, T. Henderson, D. Ranasinghe, V. G. Zakrzewski, J. Gao, N. Rega, G. Zheng, W. Liang, M. Hada, M. Ehara, K. Toyota, R. Fukuda, J. Hasegawa, M. Ishida, T. Nakajima, Y. Honda, O. Kitao, H. Nakai, T. Vreven, K. Throssell, J. A. Montgomery Jr., J. E. Peralta, F. Ogliaro, M. J. Bearpark, J. J. Heyd, E. N. Brothers, K. N. Kudin, V. N. Staroverov, T. A. Keith, R. Kobayashi, J. Normand, K. Raghavachari, A. P. Rendell, J. C. Burant, S. S. Iyengar, J. Tomasi, M. Cossi, J. M. Millam, M. Klene, C. Adamo, R. Cammi, J. W. Ochterski, R. L. Martin, K. Morokuma, O. Farkas, J. B. Foresman and D. J. Fox, Gaussian 16 Rev. B.01, Wallingford, CT, 2016.

19 a) A. D. Becke, *J. Chem. Phys.*, 1993, **98**, 5648; b) Lee, Yang and Parr, *Phys. Rev. B: Condens. Matter*, 1988, **37**, 785;

20 a) F. Weigend and R. Ahlrichs, *PCCP*, 2005, **7**, 3297; b) F. Weigend, *PCCP*, 2006, **8**, 1057;

21 J. P. Merrick, D. Moran and L. Radom, *J. Phys. Chem. A*, 2007, **111**, 11683.

22 a) P. Buday, C. Kasahara, E. Hofmeister, D. Kowalczyk, M. K. Farh, S. Riediger, M. Schulz, M. Wächtler, S. Furukawa, M. Saito, D. Ziegenbalg, S. Gräfe, P. Bäuerle, S. Kupfer, B. Dietzek-Ivanšić and W. Weigand, *Angew. Chem. Int. Ed.*, 2022, **61**, e202202079; b) H. Abul-Futouh, Y. Zagranyarski, C. Müller, M. Schulz, S. Kupfer, H. Görls, M. El-khateeb, S. Gräfe, B. Dietzek, K. Peneva and W. Weigand, *Dalton Trans.*, 2017, **46**, 11180; c) P. Buday, P. Seeber, C. Zens, H. Abul-

Futouh, H. Görls, S. Gräfe, P. Matczak, S. Kupfer, W. Weigand and G. Mloston, *Chem. Eur. J.*, 2020, **26**, 11412; d) P. E. M. Siegbahn and R.-Z. Liao, *J. Phys. Chem. A*, 2020, **124**, 10540;

23 a) B. Mennucci, C. Cappelli, C. A. Guido, R. Cammi and J. Tomasi, *J. Phys. Chem. A*, 2009, **113**, 3009; b) A. V. Marenich, C. J. Cramer and D. G. Truhlar, *J. Phys. Chem. B*, 2009, **113**, 6378;

24 S. Grimme, S. Ehrlich and L. Goerigk, *J. Comput. Chem.*, 2011, **32**, 1456.

25 R. D. Johnson, *Computational Chemistry Comparison and Benchmark Database, NIST Standard Reference Database 101*, 2011.